Proceedings of the Second International Workshop on EGS, 8.-12. August 2000, Tsukuba, Japan
KEK Proceedings 200-20, pp.224-234

Implementation and Performance Evaluation of Iterative Reconstruction Algorithms in SPECT: A Simulation Study Using EGS4

T. Yokoi[1], H. Shinohara[2], T. Hashimoto[3], T. Yamamoto[4], and Y. Niio[4]

[1] *Department of Research and Development for Nuclear Medicine, Shimadzu Corporation, Kyoto, Japan*
[2] *Department of Radiological Sciences, Tokyo Metropolitan University of Health Sciences, Tokyo, Japan*
[3] *Department of Information Processing, Yokohama Soei College, Yokohama, Japan*
[4] *Department of Radiology, Showa University Fujigaoka Hospital, Yokohama, Japan*

Abstract

We implemented three iterative reconstruction algorithms (maximum likelihood-expectation maximization (MLEM) algorithm, multiplicative simultaneous iterative reconstruction technique (MSIRT) and additive simultaneous iterative reconstruction technique (ASIRT)) incorporating attenuation correction (AC) and scatter correction (SC) for single photon emission computed tomography (SPECT). The purpose of this study is to investigate the convergence properties of the three iterative methods by computer simulation using EGS4. Digital brain and cyrindrical phantoms were designed for activity distribution and linear attenuation coefficient maps. In this study, the simulated radioisotope was Tc-99m (photon energy = 140keV). The photon attenuation and scatter and the distance-dependent blurring due to the collimator were involved in the simulated SPECT system. In the implemented reconstruction algorithms, modeling of the effect of attenuation and scattering were involved but the distance-depend blurring was not included. The progress of the reconstruction was monitored by observing the residual squares error (χ^2) between the calculated projections and measurement data at each iteration.

The number of iterations needed to reach a constant χ^2 value were different for each algorithm. ASIRT needed the largest number, MLEM the lowest number of iteration. The ASIRT required more than 100 iteration to produce a comparable result of MLEM and MSIRT. We observed almost equivalent performance between MLEM and MSIRT. All iterative reconstruction algorithms were effective in compensating for non-uniform attenuation distribution. There are potential in the iterative reconstruction algorithms for improvement of quantitative SPECT capability. EGS4 is powerful tool for investigating the properties of reconstruction algorithms without actual phantom experiments using the radioactive isotopes.

1 Introduction

Many iterative reconstruction algorithms for single photon emission computed tomography (SPECT) have been proposed[1-4]. One of the most important issues in SPECT is quantitative accuracy of radionuclide distributions and concentrations. The concentration of the tracer gives physiological information about the metabolism of a living tissue. The advantage of the iterative reconstruction algorithms is that they can easily incorporate a model of the physical processes influencing the absolute quantitation, such as photon attenuation and scatter in organ [5]. In SPECT, the spatial resolution depends on the distance from the detector due to the finite hole-diameter of the collimator. The compensation of the distance-dependent blurring can be also included into the algorithm [4]. Therefore the iterative reconstruction algorithms are expected to improve the quantitative capability

of SPECT. These methods have long been considered not to be suitable in clinical routine studies due to the excessive computational requirement of each iteration step and slow convergence. Because of increases in computer power, the iterative reconstruction for SPECT has recently become clinically available as an alternative to conventional filtered backprojection algorithm.

We implemented three iterative reconstruction algorithms, maximum likelihood-expectation maximization (MLEM) algorithm [1,2], multiplicative simultaneous iterative reconstruction technique (MSIRT)[3,6] and additive simultaneous iterative reconstruction technique (ASIRT)[3], incorporating the attenuation and scatter compensation for SPECT. The choice of the algorithm and selecting of a stopping iteration number depend on the conditions in a given clinical environment. The object of this study is to investigate the convergence properties of the iterative reconstruction algorithms using EGS4 [7].

2 Theory of Iterative Reconstruction Algorithms

2.1 Definition of notation

Figure 1 shows the notation and coordination system for the reconstruction. λ_j^k is the value of reconstructed image at the pixel j for the k-th iteration, y_i is the measured projection data at i-th bin, and C_{ij} is the detection probability that give the fraction of photons from pixel j to projection bin i. The value of C_{ij} represents as the overlapped area between i-th ray tube and pixel j.

2.2 Iterative reconstruction algorithms

Maximum likelihood-expectation maximization (MLEM) algorithm is described as follows:

$$\lambda_j^{k+1} = \frac{\lambda_j^k}{\sum_i^m C_{ij}} \sum_i^m \frac{C_{ij}}{\sum_j^m C_{ij}\lambda_j^k} \tag{1}$$

where k is the iteration number. This algorithm converges to the maximum likelihood estimate of a probability distribution function from the observed data [8]. In this algorithm, the measured emission data is assumed a spatially dependent Poisson model.

Additive simultaneous iterative reconstruction technique (ASIRT) and multiplicative simultaneous iterative reconstruction technique (MSIRT) are described as follows, respectively:

$$\lambda_j^{k+1} = \lambda_j^k + \frac{1}{\sum_i^m C_{ij}} \sum_i^m \frac{(y_i - \sum_j^m C_{ij}\lambda_j^k)C_{ij}}{\sum_j^m C_{ij}} \tag{2}$$

$$\lambda_j^{k+1} = \lambda_j^k \frac{\sum_i^n (C_{ij} y_i / \sum_j^m C_{ij})}{\sum_i^n (\sum_j^m C_{ij}\lambda_j^k / \sum_j^m C_{ij})} \tag{3}$$

In ASIRT and MSIRT methods, the measured emission data is assumed a Gauss distribution. Figure 2 show the flowcharts of each algorithm. The reconstruction images are iteratively upgraded by the different manners. All algorithms must be started from positive initial estimates of λ^0, and the C_{ij} is calculated at once before the iteration cycle. There is no mathematical rule for stopping of the iteration, so it must be found empirically.

2.3 Incorporation of attenuation and scatter correction into the algorithms

The effect of photon attenuation can be easily incorporated into the probability C_{ij}. The number of photons are exponentially decreased passing through a pixel j. The attenuation factor is given by $\exp(-\sum_{j \in J_i} \mu_j l_{ij})$, where μ_j is the linear attenuation coefficient [cm^{-1}] at the pixel j, J_i is the subset of pixels passing through the i-th ray and l_{ij} is the intersection length [cm]. The μ_j map is supplied as a prior information measured by the external radioisotope source or X-ray CT scanner. The

probability incorporating the attenuation consists in calculating $C_{ij}\exp(-\sum_{j\in J_i}\mu_j l_{ij})$. In practical implementation, the value of was approximated by C_{ij} x [pixel size].

The scatter component contaminated in the main window was approximated by the method of Ogawa et al [9,10]. This method was assumed that the scatter component could be calculated by linear interpolation using the images of sub-window as follows:

$$S_i = 0.5\frac{C_{S_i}}{W_s}W_m \tag{4}$$

where C_{S_i} is the measured counts in the sub-window at i-th bin, W_s and W_m are the width of sub- and main- window [keV], respectively. In order to incorporate the scatter correction, the estimated scatter component S_i was subtracted from the measured projection data y_i in each algorithm. Including the above-mentioned procedures, the attenuation correction (AC) and scatter correction (SC) can be accomplished. Although the blurring due to the solid angle of the collimator hole was included in the simulation data, it was not included in the reconstruction algorithms.

3 Simulation

3.1 Digital phantoms and material data

To evaluate the properties of the implemented iterative reconstruction algorithms, we performed the simulation study using the digital brain and cylindrical phantoms as shown in Fig.3. In the brain phantom, the activity distribution map was modeled as the gray and white matter structures segmented from autopsy brain phantom [11]. The activity ratio of gray/white matter was assumed to 4:1. The linear attenuation coefficient map consisted of brain tissue and skull regions. The component of the brain tissue was assumed to equivalent of the water (H_2O). On the other hand, the skull region that has no activity consisted of six elements from H, C, N, O, P, and Ca. These data were supplied into the PEGS program to produce the material file that contained the cross section of interaction. In this study, the simulated radioisotope was Tc-99m (photon energy = 141keV). The linear attenuation coefficients μ for the narrow beam of 141 keV were estimated about 0.15 and 0.26 cm^{-1} for tissue and skull, respectively. The cylindrical phantom was defined as the same fashion but a uniform activity distribution was assumed. The phantoms were a 128 x 128 matrix with a pixel size of 3.125 mm.

3.2 Generation of projection data using EGS4

The photons were generated using EGS4 [7] and user extended program for a SPECT system coded by Narita et al. [12,13]. The codes were implemented into the Windows based computer (Pentium-III, 600MHz, 128MB) by Visual Fortran Ver 6.1(Compaq Corp.). The digital phantoms and the pre-calculated material file by PEGS were supplied into the EGS4 program. The physical processes of attenuation, scatter and the blurring due to the detector response were involved in the simulated SPECT system. Two kinds of collimator (ultra high-resolution type (UHR) and high-sensitive type (HS)) were examined. The parameters used in the simulation were summarized in Table 1.

3.3 Convergence criteria

To investigate the convergence properties of the implemented iterative algorithms, two criteria have been examined. First the progress of the reconstruction was monitored by observing the residual squares error (χ^2) at each iteration. χ^2 is defined as follows:

$$\chi^2 = \sum_i^m (p\_y_i) \tag{5}$$

χ^2 is interpreted that how well the forward projection of the image matches with the measured data. Therefore it will be expected to decrease with increasing the iteration number, and approach to the

plateau. Secondly, evaluating of gray/white count ratio also monitored the image contrast. The regions of interest (ROI) were defined on the deep gray matter and white matter by 3 x 3 square pixels. The gray/white ratio will be approach to the assumed value of 4.0 if the AC, SC and compensation of blurring by collimator are perfect.

4 Results and Discussion

The simulated energy spectra of Tc-99m using the UHR collimator and the brain phantom are shown in Fig.4. The defined energy windows are also indicated on the same figure. The primary spectrum, which cannot be measured in actual experiment, represents that photon experience no interaction passing through the organ. The total spectrum is summation of the primary and scatter. The estimated energy spectra were similar with the results of previous report of simulation study [14].

Fig.5 shows the progress of reconstructed images of cylindrical phantom using MLEM algorithm and the HS collimator as function of the iteration number. χ^2 decreased rapidly at early iterations. Subsequently it declines slightly at late iterations. In this case, the feasible iteration number could be determined as about 40 iteration for with attenuation and scatter correction (ACSC) and 30 iteration for without ACSC. The values of χ^2 performed by AC and SC were small compared to those without correction. The same tendency was observed in the results using UHR. The computation time for image reconstruction was about 2 sec for one iteration.

Fig.6 shows the generated sinogram (projection data) from brain phantom and reconstructed images using MLEM with and without ACSC for both collimators. The maximum counts in the projection data of main window were 17805 and 1811 counts/pixel using HS and UHR, respectively. The sensitivity of HS was about 10 times higher than that of UHR. The computation times for generating of the sinograms were about 10 hr and 16 hr using HS and UHR, respectively. The values of χ^2 using MLEM algorithm with and without ACSC are shown in Fig.7 as a function of the number of iteration. The reconstructed images at each iteration were also shown. The feasible iteration numbers were about 40 for HS and 50 for UHR when AC and SC were performed. Visual inspection has confirmed that the stopping rule work well. It is evident that the performing of AC and SC slows the iterative process down. Fig.8 shows the comparison of three algorithms on χ^2 with ACSC. The number of iterations needed to reach a constant value were different for each algorithm. ASIRT needed the largest number, MLEM the lowest number of iteration. The ASIRT required more than 100 iteration to produce a comparable result of MLEM and MSIRT. We observed almost equivalent performance between MLEM and MSIRT. The similar results were obtained using HS.

Fig. 9 shows the count ratio of gray and white matter in ROIs as a function of the iteration number using MLEM. By performing the AC and SC, the gray/white ratio was improved from 1.99 to 2.89 using HS and 2.89 to 3.82 using UHR at 80 iteration. In UHR collimator study, the estimated gray/white values were nearly equal to the assumed value of 4.0, but a little underestimation (-4.5%) was observed. The reasonable explanation for the underestimation is that modeling of distance-dependent blurring was not included in the reconstruction algorithms. Fig.10 shows the comparison of algorithms on gray/white ratio using UHR collimator. All iterative reconstruction algorithms were effective in compensating for scatter and non-uniform attenuation distribution. The simulations revealed the slow convergence property of ASIRT. It also makes little different on the results whether we utilize MLEM or MSIRT for the image reconstruction.

5 Conclusion

We implemented three iterative reconstruction algorithms incorporation of scatter and attenuation compensation. In order to investigate the convergence properties, the simulation SPECT system using EGS4 was constructed. The simulation studies makes clear convergence properties of each algorithm for two kinds of phantoms and collimators. In conclusion, these methods are potential for

improvement of quantitative SPECT capability. EGS4 is powerful tool for investigating the properties of reconstruction algorithms without actual phantom experiments using the radioactive isotopes.

Acknowledgment

We thank to Dr. Yuichiro Narita of Chiba Cancer Center for providing the projection program and helpful suggestion for EGS4.

References

[1] L. Shepp and Y. Vardi, "Maximum likelihood reconstruction for emission tomography". *IEEE Trans. Med. Imaging* **MI-1**(1982)113-122.

[2] K. Lange and R. Carson, "EM reconstruction algorithms for emission and transmission tomography", *J. Comput Assist Tomogr* **8**(1984)306-316.

[3] P. Gilbert, "Iterative methods for the three-dimensional reconstruction of an object from projections", *J. Theor. Biol.* **36**(1972)105-117.

[4] B. M. W. Tsui, X. Zhao, E. C. Frey, G. T. Gullberg. "Comparison between ML-EM and WLS-CG algorithms for SPECT image reconstruction", *IEEE Trans Med Imaging* **MI-13**(1994)601-609.

[5] S. Mastuoka, H. Shinohara, S. Yamamoto, Y. Niio, H. Shima, M. Yamada, et al., "Combined scatter and attenuation correction for Tl-201 myocardial perfusion SPECT using OS-EM algorithm", *Nippon Acta Radiologica* **58**(1998)751-757.

[6] DM Titterington, "On the iterative image space reconstruction algorithm for ECT", *IEEE Trans. Med. Imaging* **MI-6**(1987)52-56.

[7] W. R. Nelson, H. Hirayama, D. W. O. Rogers, "The EGS4 code system", Stanford Linear Accelerator Center Report *SLAC-265*, 1985.

[8] A. P. Dempster, N. M. Laird, D. B. Rubin, "Maximum likelihood from incomplete data via the EM algorithm", *J. Roy Statis Soc* **B39**(1977)1-38.

[9] K. Ogawa, Y. Harata, T. Ichihara, A. Kubo, S. Hashimoto, "A practical method for position-dependent Compton-scatter correction in single photon emission CT", *IEEE Trans. Med. Imag.* **10**(1991)408-412.

[10] T. Ichihara, H. Maeda, K. Yamakado, N. Motomura, K. Matsumura, K. Takeda, T. Nakagawa, "Quantitative analysis of scatter- and attenuation-compensated dynamic single-photon emission tomography for functional hepatic imaging with a receptor-binding radiopharmaceutical", *Eur. J. Nucl. Med.* **24**(1997)59-67.

[11] G. Salamon and Y. P. Huang,"Computed tomography of the brain", Springer-Verlag, Berlin Heidelberg New York, 1980.

[12] H. Iida, Y. Narita, S. Eberl, "Simulation of Compton scatter in single photon-emission computed-tomography", Fifth EGS4 User's Meeting in Japan, *KEK Proceedings 95-9*, 33-46, 1995.

[13] Y. Narita, H. Iida, S. Eberl, et al., "Monte Calro evaluation of accuracy and noise properties of two scatter correction methods for ^{201}Tl cardiac SPECT", *IEEE Trans. on Nucl. Sci.* **44**(1997)2465-2472.

[14] S. Maeda, K. Ogawa, "Quantitative assessment of scattered photons considering skull bone in brain SPECT", *Jpn. J. Nucl. Med. (Kaku-Igaku)* **31**(1994)431-439.

Table 1. Simulation parameters

Detector size	400 mm x 250 mm
Collimator geometry	
Ultra high resolution (UHR)	1.0 mm ϕx 60 mm
High sensitive (HS)	2.0 mm ϕx 35 mm
Scintillator material and thickness	NaI(Tl), 9.5mm
Energy windows	
Main window	141 keV $\pm$ 10%
Sub window	120 keV $\pm$ 5%
Energy resolution	10%
Rotation radius	250 mm
Projection	128 x 128 matrix, 128 views over 360 degree
Pixel size	3.125 mm

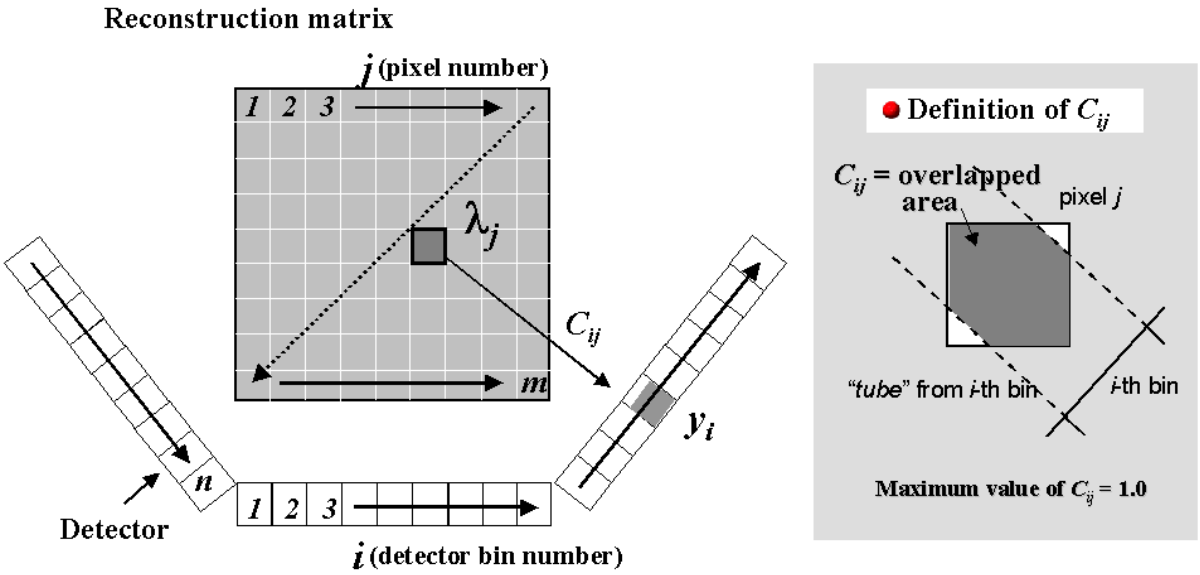

Figure 1: Notation and coordinate systems

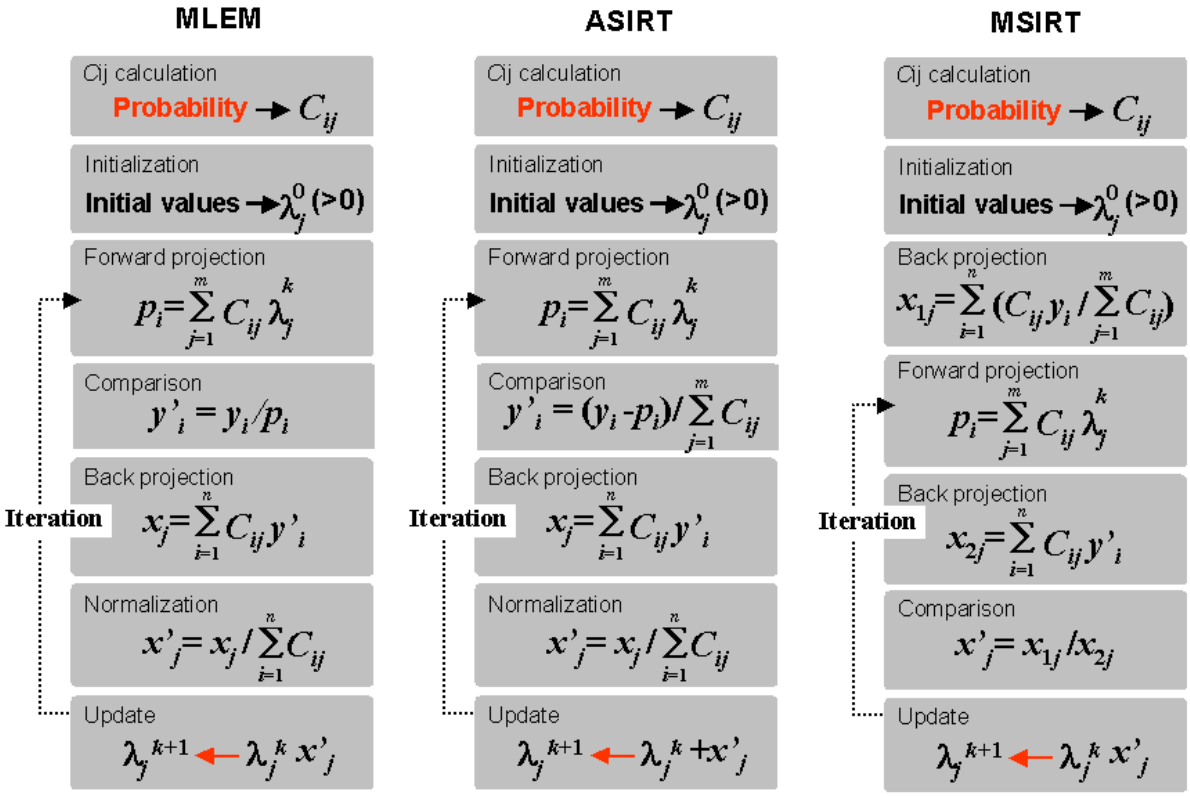

Figure 2: Flowchart of three iterative algorithms.

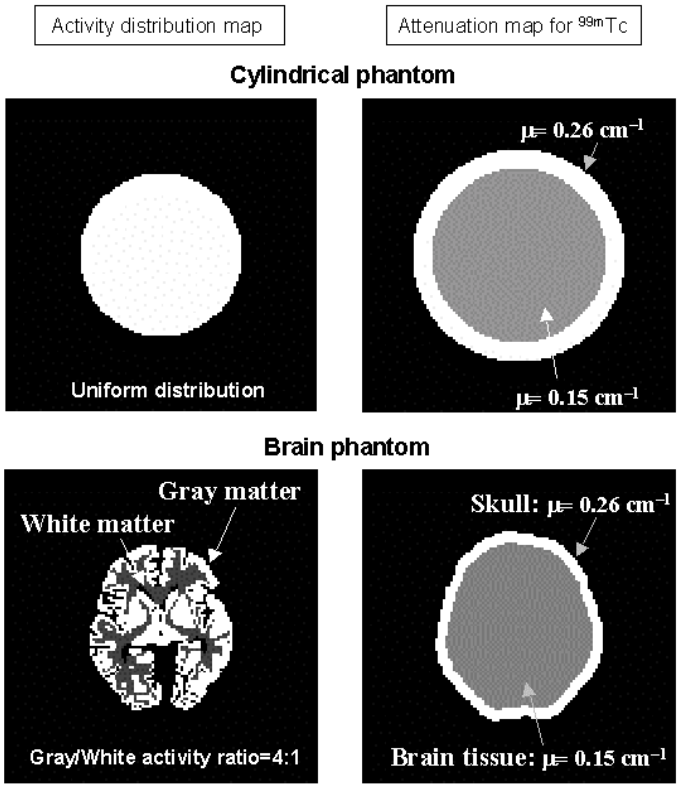

Figure 3: Digital cylindrical and brain phantoms used in the simulation.

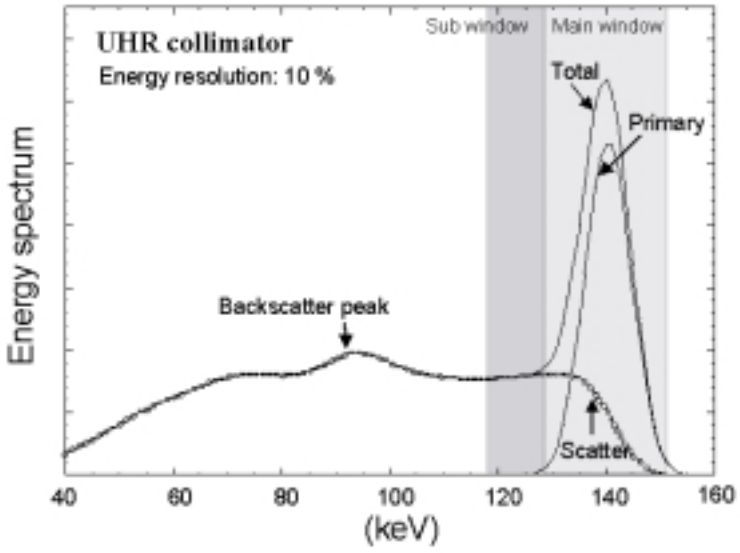

Figure 4: Simulated energy spectra using EGS4.

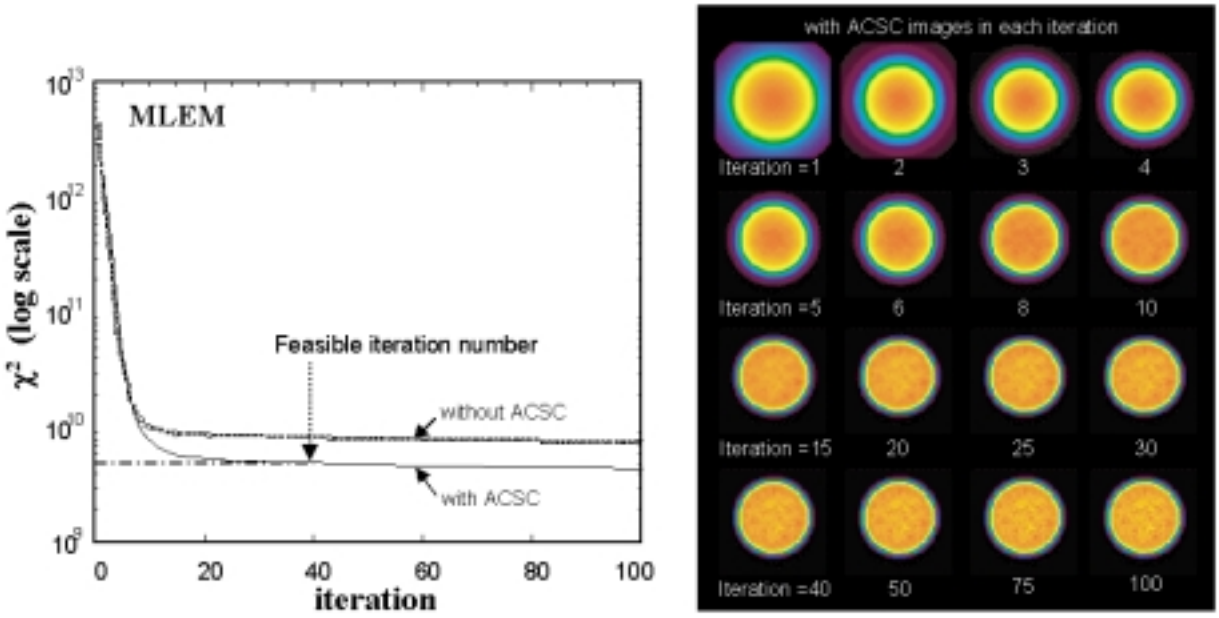

Figure 5: Progress of reconstruction for the cylindrical phantom using MLEM algorithm as a function of iteration number.

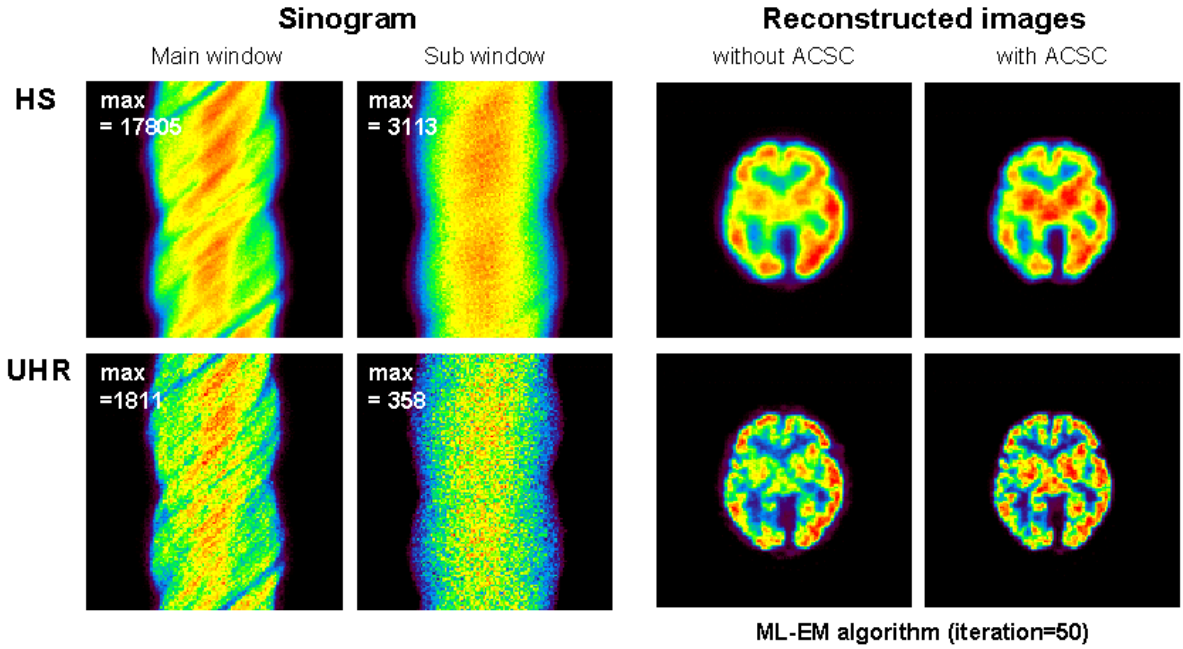

Figure 6: The generated sinograms (projection data) from brain phantom and reconstructed images using MLEM with and without ACSC for both collimators.

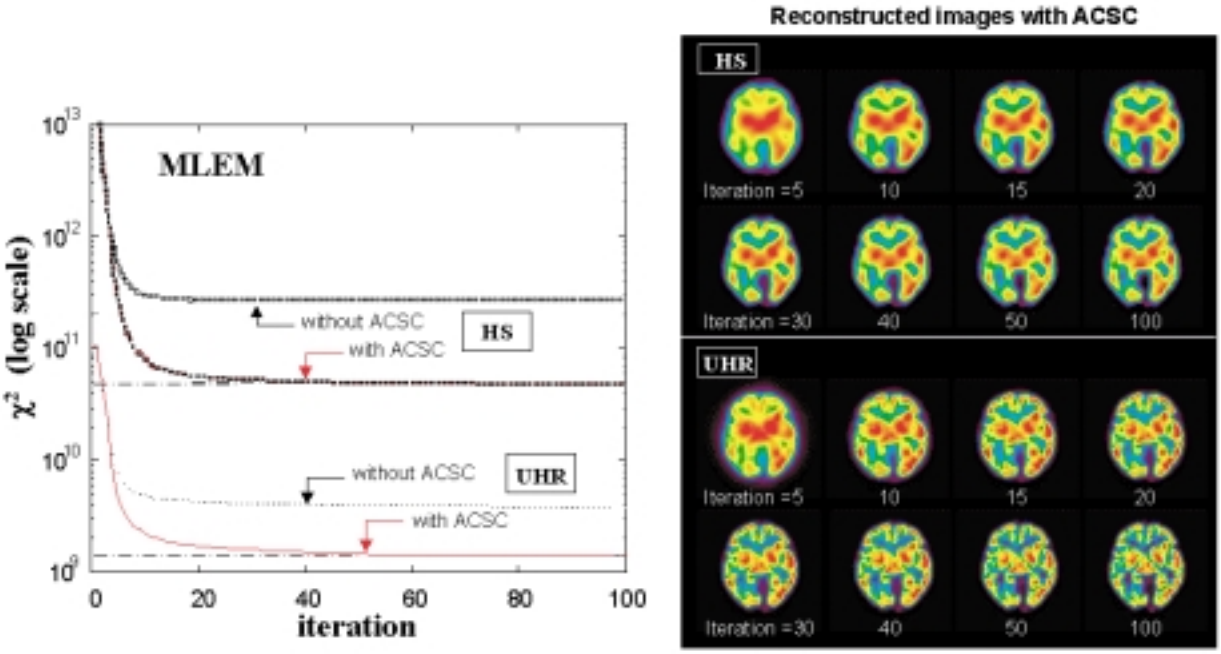

Figure 7: The values of χ^2 using MLEM algorithm with and without ACSC as a function of the number of iteration.

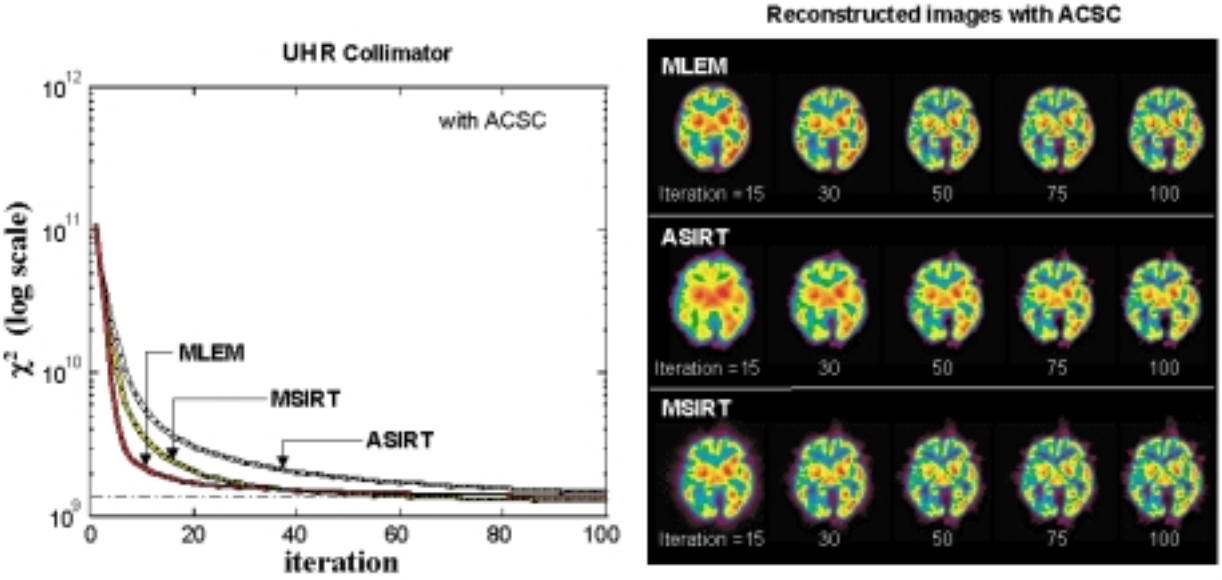

Figure 8: Comparison of three iterative algorithms on χ^2 using UHR collimator as a function of the number of iteration.

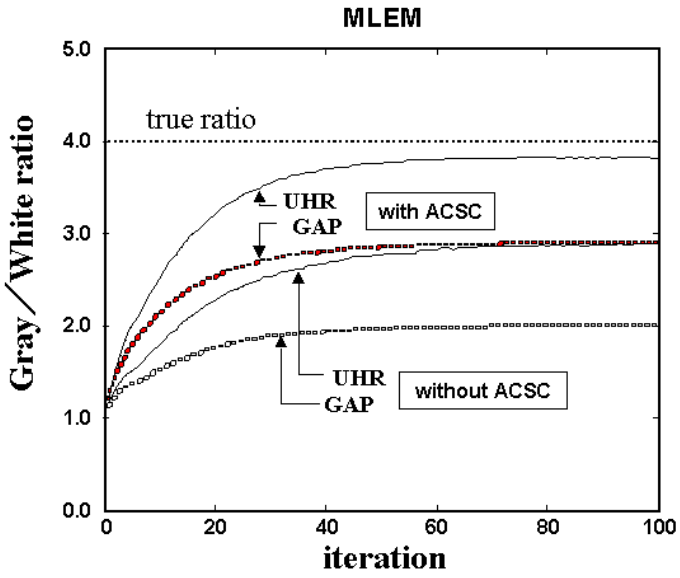

Figure 9: The values of gray/white matter counts ratio using MLEM algorithm with and without ACSC as a function of the number of iteration.

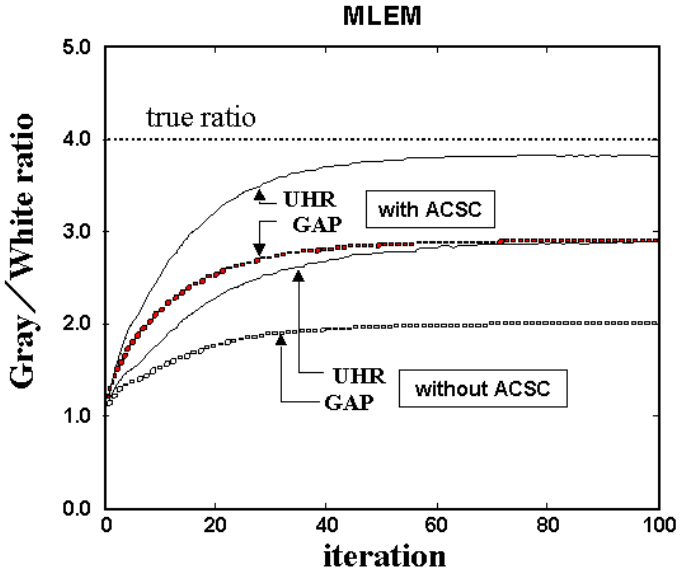

Figure 10: Comparison of three iterative algorithms on gray/white matter counts ratio using UHR collimator as a function of iteration.